PROBLEMY MECHATRONIKI
UZBROJENIE, LOTNICTWO, INŻYNIERIA BEZPIECZEŃSTWA

PROBLEMS OF MECHATRONICS
ARMAMENT, AVIATION, SAFETY ENGINEERING

ISSN 2081-5891; E-ISSN 2720-5266 **https://promechjournal.pl/**

Dynamic Behaviour of Selective Laser Melted 316L Steel - Mechanical Properties and Microstructure Changes

Paweł BIAŁOBRZEWSKI (pawel.bialobrzewski@student.wat.edu.pl)
Judyta SIENKIEWICZ* (judyta.sienkiewicz@wat.edu.pl)
Jacek JANISZEWSKI (jacek.janiszewski@wat.edu.pl)
Janusz KLUCZYŃSKI (janusz.kluczynski@wat.edu.pl)

*Corresponding author
ORCID: https://orcid.org/0000-0001-5372-1862

Military University of Technology,
Faculty of Mechatronics, Armament and Aerospace,
Institute of Armament Technology
2 Sylwestra Kaliskiego Str., 00-908 Warsaw, Poland

Received: July 7, 2022 / Revised: August 2, 2022 / Accepted: August 29, 2022 / Published: June 30, 2023.

2023, 14 (2), 51-72**;** https://doi.org/10.5604/01.3001.0053.6671

Cite: Chicago Style

Białobrzewski, Paweł, Judyta Sienkiewicz, Jacek Janiszewski, and Janusz Kluczyński. 2023. "Dynamic Behaviour of Selective Laser Melted 316L Steel - Mechanical Properties and Microstructure Changes". *Probl. Mechatronics. Armament Aviat. Saf. Eng.* 14 (2): 51-72. https://doi.org/10.5604/01.3001.0053.6671

Abstract. 316L steel specimens with three different shear zones made by SLM (Selective Laser Melting) were subjected to dynamic tests using the Split Hopkinson Pressure Bar method. The effect of high-speed deformation on changes in microstructure was analyzed. In addition, the stress-strain relationship was determined from the SHPB results. To visualize the deformation process of the specimens during the tests, a camera with a high frame rate was used. It was shown that as the plastic deformation increases, the hardness of the material increases. Microstructural analysis of dynamically loaded areas revealed numerous defects. Twinning was found to be the main deformation mechanism. Large plastic deformation and many other microstructural changes such as shear bands, cracks and martensite nucleation were also observed.
Keywords: microstructure, stainless steel, selective laser melting, additive manufacturing, split Hopkinson pressure bar

1. INTRODUCTION

Additive manufacturing (AM), also known as "3D printing" is a process of building objects by successive addition of material, usually layer by layer, based on 3D computer-aided design (CAD) models. The first devices using this technology were developed in the 1980s. Originally, they were used only for easy and quick prototyping, however, as the technology developed, it became possible to print final components with properties similar to those achieved by conventional methods. Nowadays, it is one of the most rapidly growing manufacturing methods, and with technological development, more potential applications will be available.

Additive methods provide unique opportunities that are often lacking in conventional manufacturing techniques, such as machining, metal forming or casting. The major advantage of additive methods is the ability to produce parts with very complex shapes, often impossible to achieve by conventional manufacturing. In many cases, it is thus possible to reduce the number of parts used, as well as the costs of their assembly, and to eliminate local weakening of material created during the joining process. Another important advantage of AM is the possibility of starting production of components right after the CAD model is created, skipping the whole procedure of designing the manufacturing process. It can reduce time and costs, especially for low-volume production or during the prototyping of a new product.

Austenitic 316L stainless steel is among the most often used and studied materials for SLM [1–5] due to its combination of good mechanical properties and excellent corrosion resistance. 316L is an optimal material for AM technology thanks to its good weldability that is associated with low carbon content (< 0.03 wt.%). Worth mentioning is that mechanical properties are strongly contingent on microstructure which in turn largely depends on the thermal history experienced during 3D printing.

The AMed microstructures generally are composed of elongated grains that are parallel to the growing directions, possessing cellular-columnar morphology that is typical for rapid cooling rates [6, 7]. Additionally, defects such as pores, incompletely melted particles, and microstructural heterogeneities are intrinsic to the AM process.

Research concerning 316L steel manufactured using SLM is mainly focused on the process parameters control and the resulting microstructure as well as material and mechanical properties, especially under static conditions [8–10].

Nonetheless, there is an open question as to how such materials behave under dynamic loading which occurs both in dynamically loaded devices as well as during high-speed machining. Therefore, in this study high strain rate test using the SHPB method has been carried out. In particular, it was shown the difference in the behaviour of AM materials under high strain rate conditions compared to static deformation. It should be pointed out that dynamic deformation studies are both technically and methodologically challenging because the results are influenced by a variety of phenomena from solid-state physics, wave propagation mechanics, thermodynamics, metrology, and materials science [11]**.**

2. TEST METHODOLOGY

2.1. Material properties

The test samples were produced via SLM from 316L steel (EN 1.4404) powder provided by LPW Technology Ltd., Widnes, UK with the chemical composition presented in Table 1. The powder grains were spherical for the most part; the diameter of the particles was in the range of 15 μm to 45 μm. The density of the material was 7.92 g/cm^3, and its flowability was 14.6 s/50 g. 316L is an austenitic stainless steel with excellent corrosion resistance and currently it is one of the most widely used alloys of stainless steel. Thanks to the addition of molybdenum, the alloy is highly resistant to atmospheric conditions and to most acids as well as to marine environments and salts. 316L can be used at elevated temperatures and it possesses good weldability while preserving high corrosion resistance at the joints. Further, the annealed alloy is non-magnetic but it can acquire magnetic properties through forming.

Table 1. Nominal ranges of contents of elements in the 316L powder (in wt%) provided by the producer.

Cr	Ni	Mo	Mn	C	P	S	Si	N	Fe
16.00 –18.00	10.00 – 14.00	2.00 – 3.00	max. 2.00	max. 0.03	max. 0.045	max. 0.03	max. 0.75	max. 0.10	Balance

2.2. Specimen preparation

Samples were produced using the SLM 125HL system provided by SLM Solutions Group AG, Lubeck, Germany. The printing process was performed with the following parameters: laser power of 150 W, exposure speed of 1000 mm/s, laser beam spot size of 70 μm, and layer thickness of 30 μm.

All specimens were fabricated under an argon atmosphere with an oxygen content of less than 0.1%. In this technology, layers of material are applied by melting powder particles using a laser beam. After creating each layer, the build platform lowers the model and another layer is fused with the previous one. Figure 1 shows the general operating principle of this technology. Components created using SLM possess very good mechanical properties and they usually require only sandblasting directly after the process. The main disadvantages are high cost and relatively low fabrication speed. The technology is used to produce parts from such materials as stainless steel, aluminium alloys, titanium, and tungsten. The microstructure of materials produced using additive manufacturing can vary depending on the technique used, as well as on the parameters of the process.

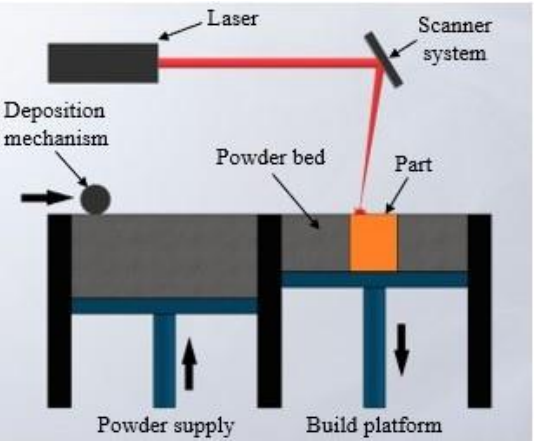

Fig. 1. The scheme of the SLM technology.

SLM manufactured samples were cylindrical with a diameter of 10 mm and length of 22 mm, see Fig. 2.

Fig. 2. 316L alloy specimens manufactured via SLM technology.

For dynamic testing, samples were cut, using a wire electrical discharge machine BP-95dn, into three variants differing in the height of the shear zone. The height of the shear zone is designed to be b_1 = 1 mm, b_2 = 0.75 mm, and b_3 = 0.5 mm to obtain three different strain rates. The geometry of the specimens is shown in Fig. 3(a). Before cutting, each specimen was ground to allow for precise fixing. After cutting each sample was sandblasted to remove any remaining chips, see Fig. 3(b) and measured using a vision measuring machine Baty Venture 2510 (Bowers Group).

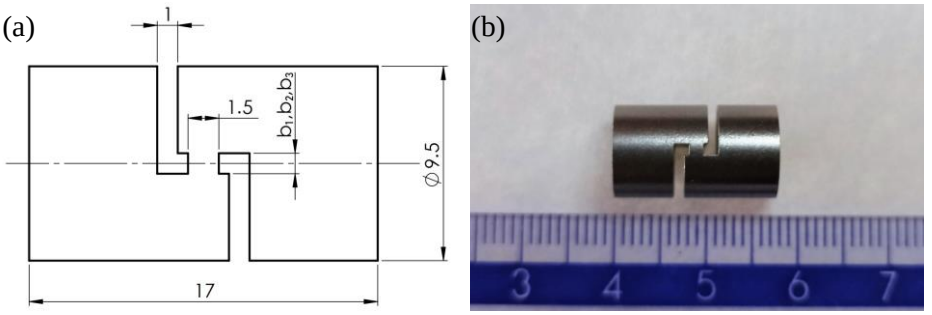

Fig. 3. (a) nominal geometry of the samples, (b) test sample after cutting and sandblasting

2.3. Test procedure

High strain rate tests were performed on a split Hopkinson pressure bar test shown in Fig. 4 [12–14]. The SHPB stand contains two main components: a transmitted bar and an incident bar, between which the sample is fixed. The striker bar fired by compressed air is used as the propulsion system. The length of the input and output bar was 1200 mm, the length of the striker bar was 250 mm, and the diameter of all bars was 12 mm. The bars were made of heat-treated maraging steel of grade MS350, providing a yield strength of 2300 MPa and an elastic wave speed of 4960 m/s.

The pulse shaping technique was used to minimise wave dispersion and facilitate stress equilibrium. A copper pulse shaper with a 3-mm diameter and thicknesses of 0.3 or 0.4 mm was used.

During the test, an elastic wave is generated in the incident bar. The wave propagating towards the specimen is fully released at the free end of the striker bar and it forms the trailing end of the incident compressive pulse strain. Once it reaches the sample interface, part of the incident wave is reflected as the reflected wave and the remaining part passes through the specimen to the transmitted bar as the transmitted wave.

The amplitude value of the wave is defined using strain gauges attached to the side surfaces of the incident and transmitted bars. The wave propagating through the bars causes deformation of the sensors, which in turn changes their electrical resistance.

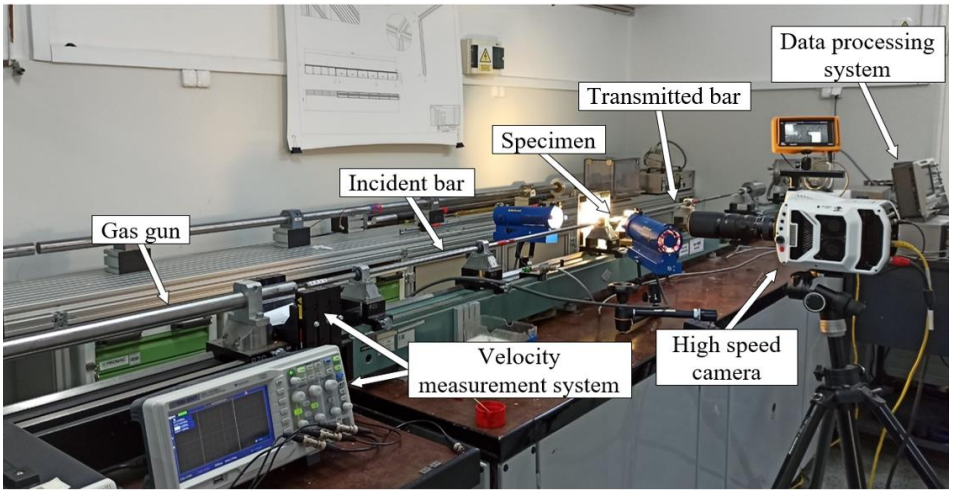

Fig. 4. Split Hopkinson pressure bar system

The wave pattern registered by strain gauges is recorded using an oscilloscope and displayed as a function of time [11].

Shear tests were performed for twelve specimens, all of them with a pressure of 2 bar. The initial striker bar velocity was about ms^{-1}, whereas the strain rates were at the level of 4.8×10^3 s^{-1}. Each test was recorded using a high-speed camera (v1612, PHANTOM, Leicester, UK), at 250000 frames per second, with a resolution of 256 × 128. The stress-strain rate response was determined using Mathcad software based on wave patterns.

For microstructural examination, before and after dynamic shear testing, samples were cut and then mounted in hot mounting bakelite resin. Next, samples were ground using sandpaper and polished with the 9 μm, 3 μm, and 1 μm diamond slurries. Final polishing has been done by using 0.25 μm silica.

The samples were electrochemically etched for 60 seconds at 15 V using a 10% aqueous oxalic acid solution. Digital light microscope Keyence VHX-6000 and scanning electron microscope (SEM) Phenom ProX equipped with energy dispersive X-ray spectrometer (EDS) with an accelerating voltage of 15 kV were used to investigate microstructural features. Porosity was measured at the bottom and top of the samples using at least 50 images. The microhardness was measured using Vickers hardness tester Qness CHD Master (Verder Scientific), with a load of 1 kgf.

3. RESULTS

3.1. Split Hopkinson pressure bar tests

One of the main purposes of conducting the SHPB test was to generate shear stress – shear strain curves of the tested material. Thus, the graphs showing the incident and reflected waves recorded by the strain gages were placed below in Fig. 5, Fig. 7, and Fig. 9. The images of tested samples with three different shear zone height widths captured during the SHPB test by a high-speed camera are shown in Fig. 6, Fig. 8, and Fig. 10. It is worth noting that plastic deformation was confined to the shear zones, while the other parts of the specimens remained elastic. For samples with the nominal shear zone height of b = 1 mm, plastic deformation was observed, but none of the specimens failed. Figure 5 shows an example of formed waves recorded by the strain gages mounted on the incident bar (red line) and transmitted bar (blue line). (Unfortunately, in the case of test 2, the data from the strain gauges was lost).

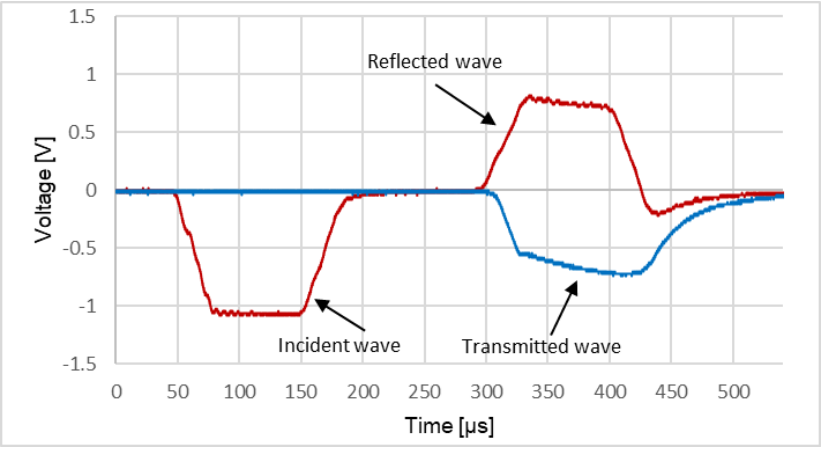

Fig. 5. Voltage versus time curve for test 1

In Fig. 6, it can be seen that the shape of the specimen shear zone changed from a true rectangular form to a parallelogram, indicating a plane shear deformation mode.

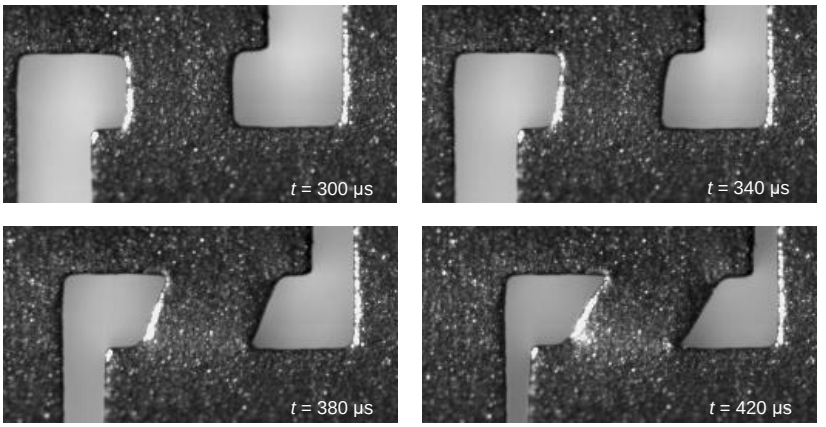

Fig. 6. High-speed camera images captured during test 1

In Fig. 7, a typical voltage versus time curve for specimens with the nominal shear zone height of b = 0.75 mm is presented. Three of the four tested samples did not crack during initial impact but they fractured at the second wave propagation. It is noticeable that at around 840 µs, the transmitted signal starts to decrease, indicating crack initiation and growth in the specimen.

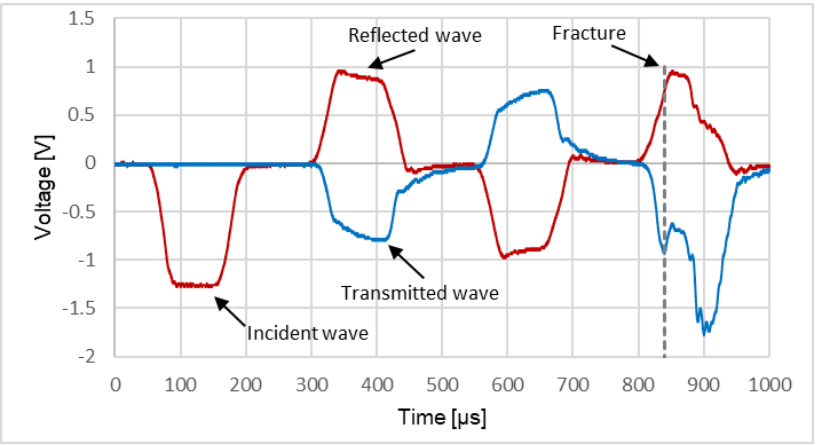

Fig. 7. Voltage versus time curve for test 5

In Fig. 8, the formation of specimen failure is shown. The crack propagates along the diagonal of the sample shear zone, dividing the specimens into two centrally symmetric parts. This phenomenon is often observed in double shear specimens and it is attributed to stress concentration at the four corners of the specimen shear zone [15–17].

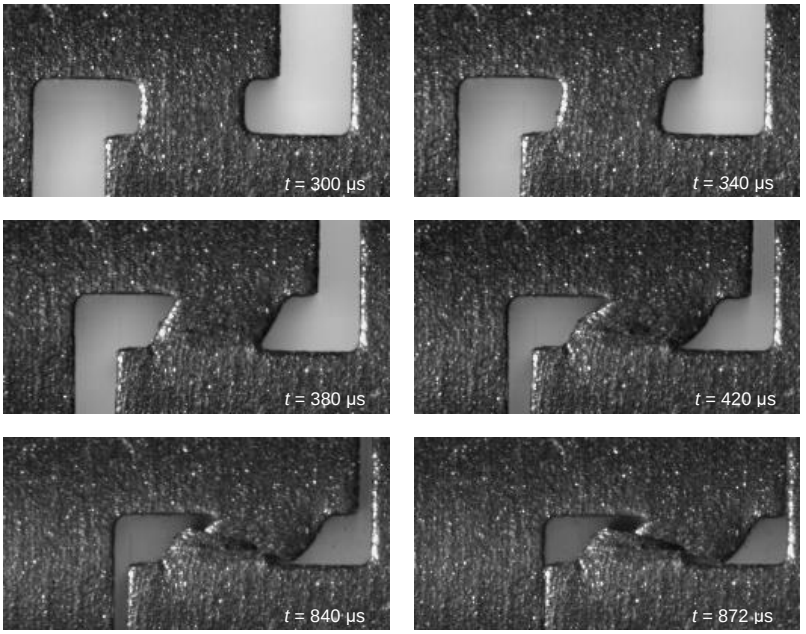

Fig. 8. High-speed camera images captured during test 5

Figure 9 represents a typical voltage signal for samples with a nominal shear zone height of b = 0.5 mm. All tested samples failed under the impact of the initial wave. It is observed at around 300 µs, that part of the incident signal begins to transfer into the tested specimen, forming the transmitted wave. After 40 µs, the transmitted signal still increases slightly while the reflected signal is almost constant. At 395 µs, the transmitted signal starts to decrease, indicating damage initiation and growth in the specimen.

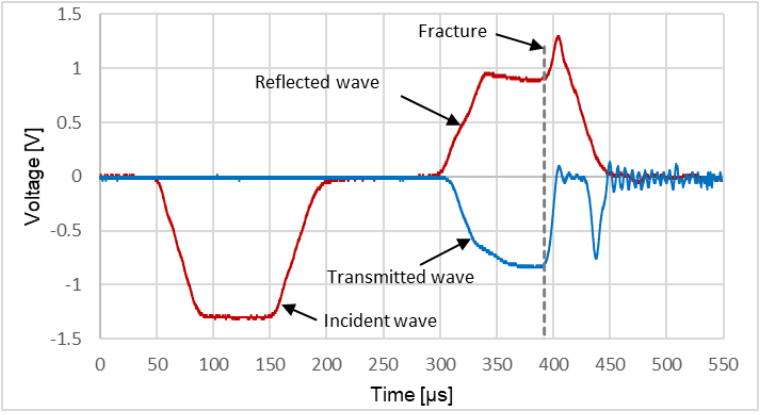

Fig. 9. Voltage versus time curve for test 9

Finally, the specimen fractures at 410 μs and at the same time the reflected signal reaches the maximum value. Figure 10 represents the failure of the specimen during the SHPB test - as in the previous cases, the crack propagated along the diagonal of the sample shear zone.

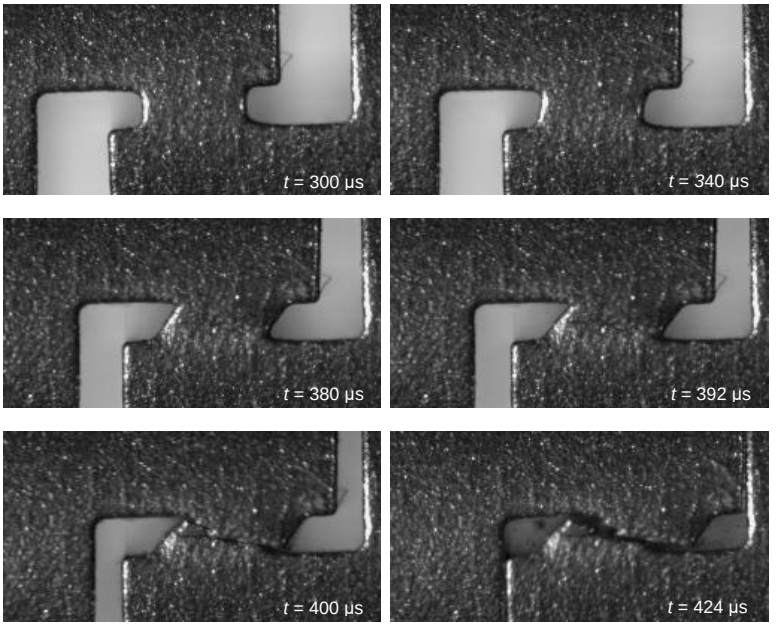

Fig. 10. High-speed camera images captured during test 9

Figure 11 (a), (b), and (c) illustrates the stress-strain curves for samples with the height of the shear zone of 1 mm, 0.75 mm, and 0.5 mm, respectively. Figure 11 (d) represents the representative characteristic of the selected sample for each set. It can be noticed that specimens with smaller shear zone experienced higher stresses, while higher strain was observed for specimens with a larger shear zone.

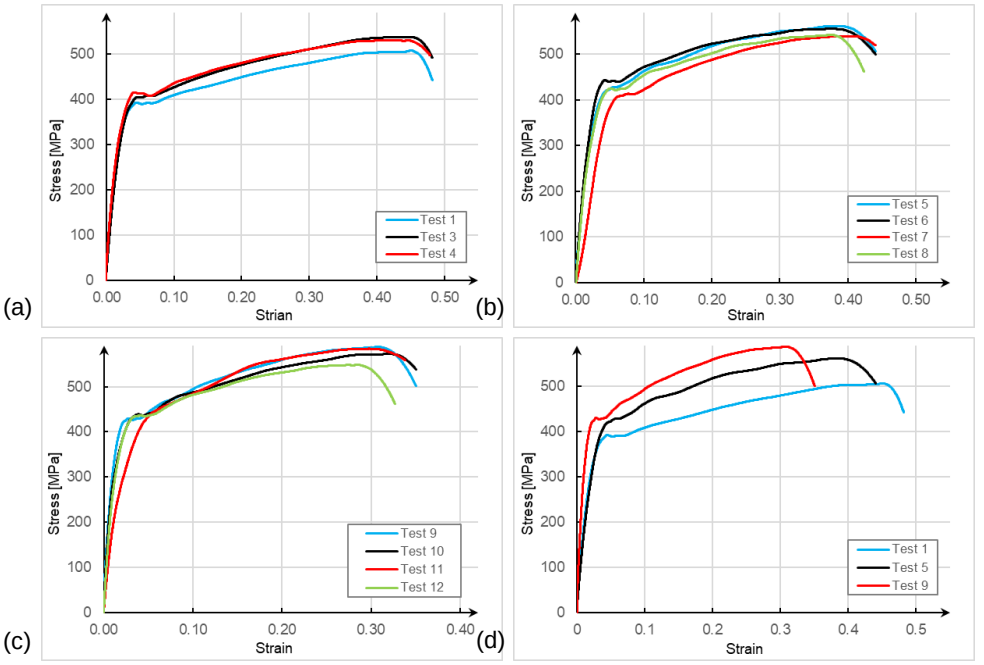

Fig. 11. Stress-strain curves for the samples with nominal shear zones: (a) 1.5 mm x 1 mm, (b) 1.5 mm x 0.75 mm, (c) 1.5 mm x 0.5 mm, (d) comparison of the representative curve for each set of samples

3.2. Microhardness

The aim of microhardness tests on as-built specimens was to highlight possible differences in microhardness induced by different cooling rates between the upper and lower parts of the SLM samples. The average microhardness of samples, manufactured via the SLM method, measured in twenty equally spaced points along the specimen axis was around 252 HV, which is significantly higher than the hardness of the 316L stainless steel manufactured conventionally in the annealed condition (max. 218 HV). The hardness measurements of SLM samples do not show substantial variations, however, the difference between the top and bottom parts was evident - the first measurement, taken in the lower part of the sample was the highest (295 HV). This may be due to higher heat dissipation during the printing process near the support material - the lower parts, are subjected to higher cooling rates.

Microhardness tests of the specimens after shear testing were performed on their axial sections within their shear zones. The measurements were conducted in the plane perpendicular to the direction of material growth. Ten measurements were made for specimen No. 1, while five measurements were made for the fractured specimens (Nos. 5 and 9). The results are presented graphically in Fig. 12.

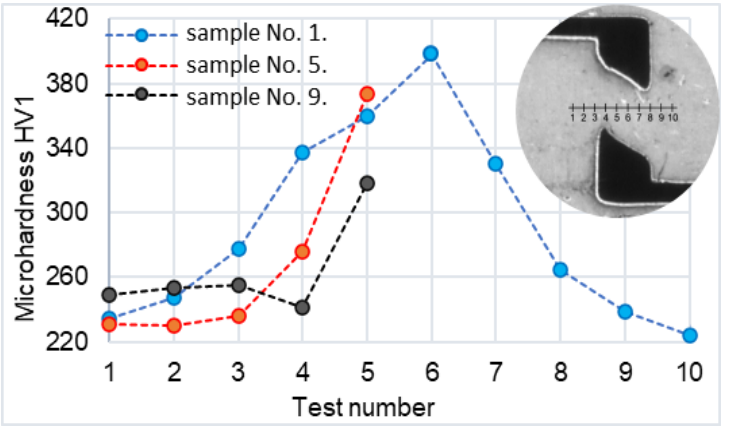

Fig. 12. Microhardness tests' results

The results show a clear increase in microhardness as the strain of the material increases. The highest measured value within the shear zone of sample No. 1 exceeds the average hardness of the material in the initial state by almost 60%. This is due to the increase in dislocation density in the material structure caused by the large plastic deformation. The maximum values recorded in the fractured samples were not as high as it was impossible to measure microhardness near the edge of the fracture.

The distance between the edge of the specimen and the centre of the indentation should be at least 2.5 times the average diagonal length of the indentation for a Vickers hardness measurement to be valid.

3.3. Chemical analysis

The results of energy-dispersive X-ray spectroscopy (EDS) are presented in Table 2. The elemental composition obtained by EDS analysis of the sample surface area is very close to the catalogue values. Only the silicon content slightly exceeds the acceptable value (1.08% with a catalogue value of 0.75%) - this may be due to inaccurate cleaning of samples after the final polishing.

Table 2. Chemical composition of the 316L powder (in wt%).

Element	Cr	Ni	Mo	Mn	Si	Fe
wt. %	17.94	12.26	2.7	1.25	1.08	64.78

Figure 13(a) shows the combined map of element distribution, while Fig. 13(b) shows the obtained X-ray spectrum. Figure 14 shows the EDS mapping of individual elements. The analysis proved that elements are not evenly distributed in the sample.

The reason may be a very high cooling rate during SLM manufacturing, which affects the uneven solidification of the melt pools.

Fluctuations in chemical composition are due to the slow kinetics of diffusion of large element atoms such as molybdenum. Local oxidation of the active elements such as chromium and silicon may be the reason for their increased content in some areas [18].

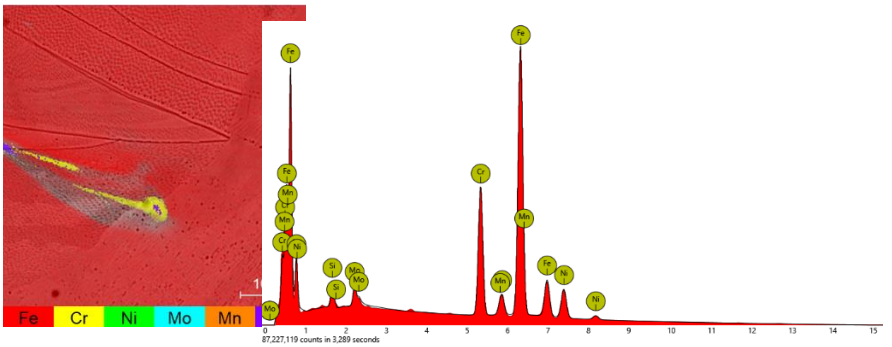

(a) (b)

Fig. 13. (a) Combined map of element distribution (b) EDS spectrometer analysis results

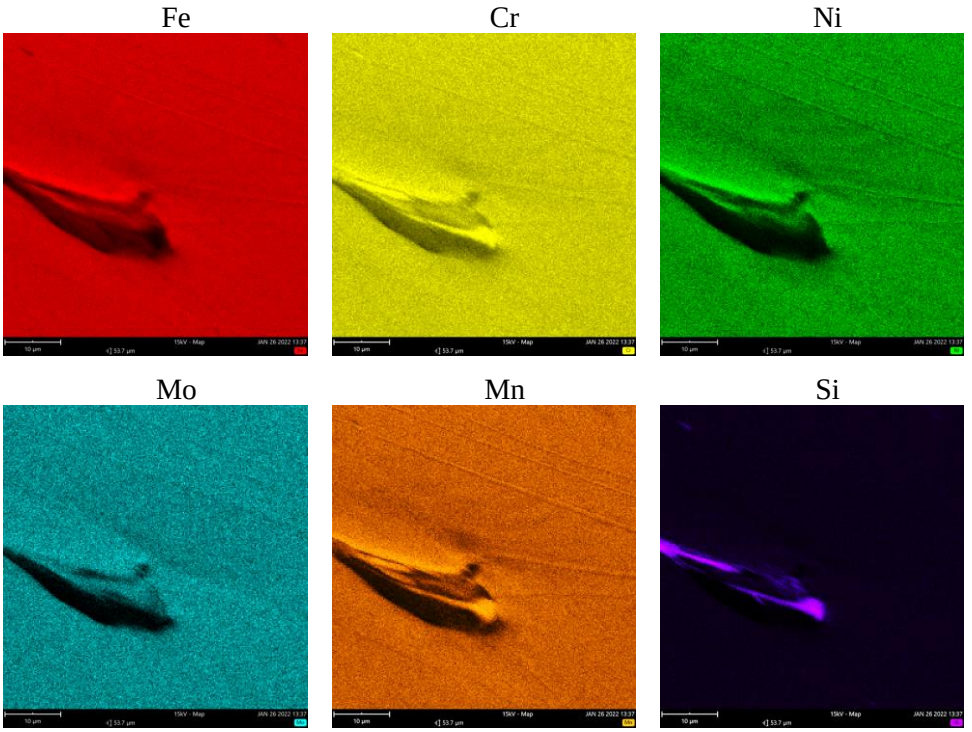

Fig. 14. EDS mapping image of SLM made 316L sample

3.4. Microstructural analysis

Images taken with a digital light microscope in a plane parallel to the material growth direction show characteristic for the SLM method structure consisting of elliptical paths formed during solidification of the melt pools, with a size of about 150 μm width and 60 μm depth, see Fig. 15(a). The images, taken in the plane perpendicular to the material growth direction, show the elongated paths generated by the laser beam pathway - Fig. 15(b).

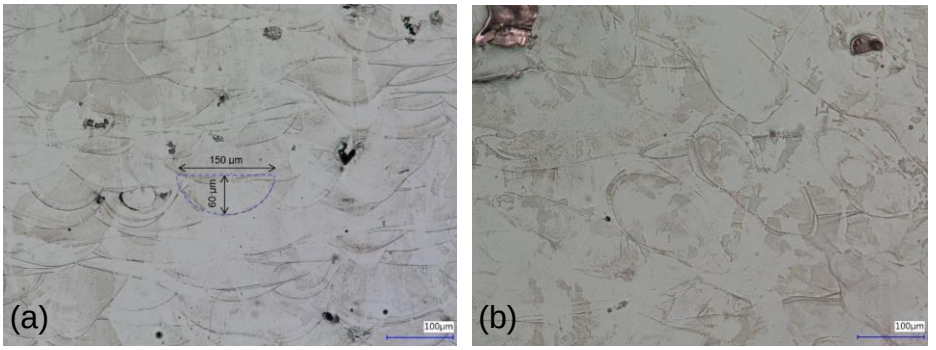

Fig. 15. Microstructure of samples in (a) longitudinal section, (b) cross-section

To compare porosity in different areas of the sample manufactured via the SLM method (bottom and top), two cross-sections were investigated, see Fig. 16.

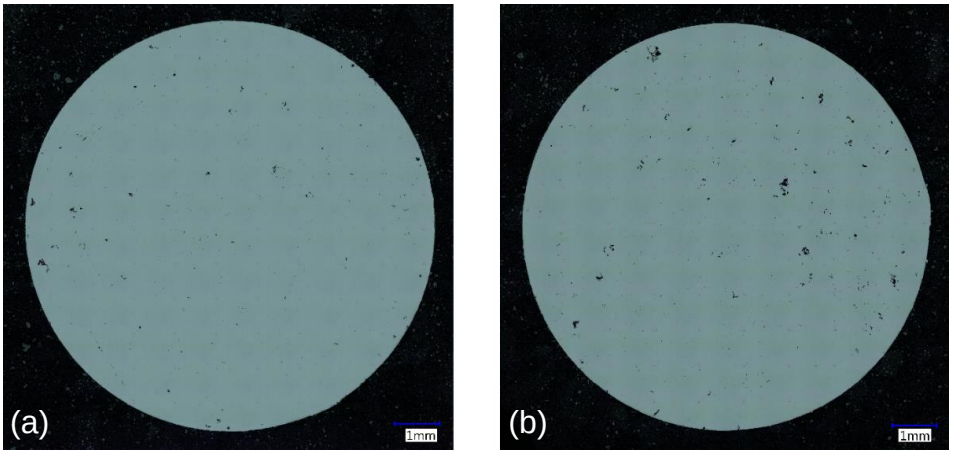

Fig. 16. Optical images of (a) lower and (b) upper cross-sections of the sample

The porosity measured in the lower part of the sample (the area where the process of printing started) was 0.3%, whereas, in the upper part of the sample, it appeared to be more than twice greater reaching the value of 0.6%.

The probable reason is the repeated heating of the lower parts of the sample during the SLM process. It is worth noting, that depending on the manufacturing process and design parameters, unique thermal histories are realisable, thus affecting the formation of pores/voids that may arise due to lack of fusion between layers, entrapped gas/debris or utilisation of porous powders. For layers at the top of the sample (further from the build plate), lack of fusion can occur due to insufficient laser power [19, 20], while for layers at the bottom (closer to the substrate) they can form, due to very high heat, transfer rates.

Examples of microstructure defects, that are characteristic of the SLM method, observed by using SEM, are presented in Fig. 17.

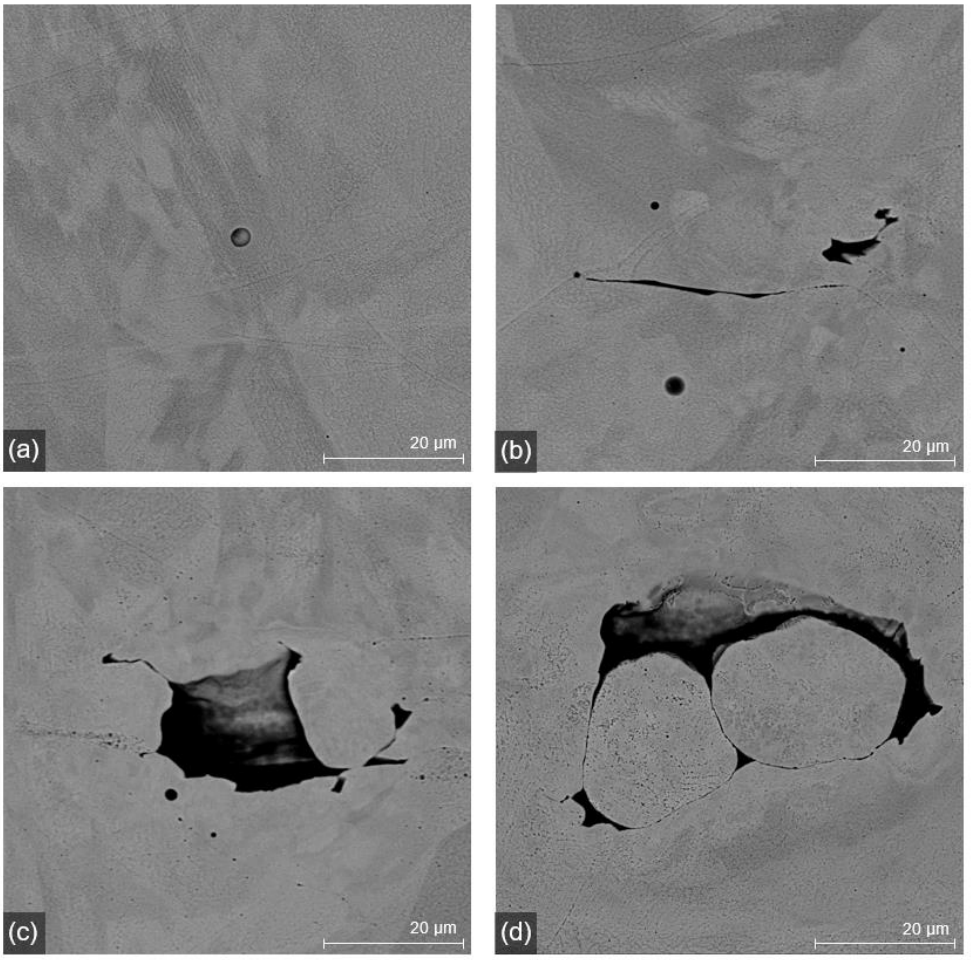

Fig. 17. Microstructure defects visible in longitudinal cross-section of SLM-produced 316L steel sample

Figure 17(a) shows an example of a pore formed by gas bubble entrapment during material solidification. The formation of such defects depends on the packing density of the powder and impurities in its chemical composition, as well as the quality of the shielding gas. Such pores are formed inside the melt pools and they are less than 10 μm in size [21]. Figure 17(b) shows a crack between the melt polls of material. The formation of such defects is due to residual stresses resulting from the rapid cooling of the material during the printing process. Figure 17(c) represents a crater formed by the incomplete melting of powder, while in Fig. 17(d) particles of unmelted powder are seen (these types of defects are usually caused by the too low energy density of the laser beam).

3.5. Microstructural characterisation of the impact–loaded areas

Microstructural changes in the samples after shear tests were investigated in their longitudinal sections, see Fig. 18 and Fig. 19.

Microstructural analysis showed that the dominant type of deformation in 316L steel, manufactured with the SLM method, is twinning - the crystal lattice of a twin creates a mirror image of the structure of the undeformed part of the material relative to a common twinning plane. Chen et al. [22] stated that the density and thickness of formed twins are closely related to the strain rate. As the strain rate increases the number of twins also increases, absorbing part of the stresses. The thickness of twins reaches its maximum at strain rates between 1000 s^{-1} - 1500 s^{-1} and further decreases with increasing strain rate.

A shear band was observed for specimen No. 1. The grains around the shear band are highly elongated and deformed, which suggests a large plastic deformation prior to the formation of the band. The observed shear band does not pass through the length of the entire section; however, these types of defects are usually preceding the formation of cracks propagating through the band.

Cracking of the material was observed in all tested specimens with the height of the shear zone of 1 mm, but only within the corners of their shear zones. Several cases of nucleation of martensite were observed in sample No. 5. As shown in [23], at low temperatures, the transformation of austenite to martensite can occur under plastic deformation at a high strain rate. The martensitic transformation in steels is non-diffusive and consists only of the reconstruction of the crystal structure from face-centred austenite to body-centred martensite.

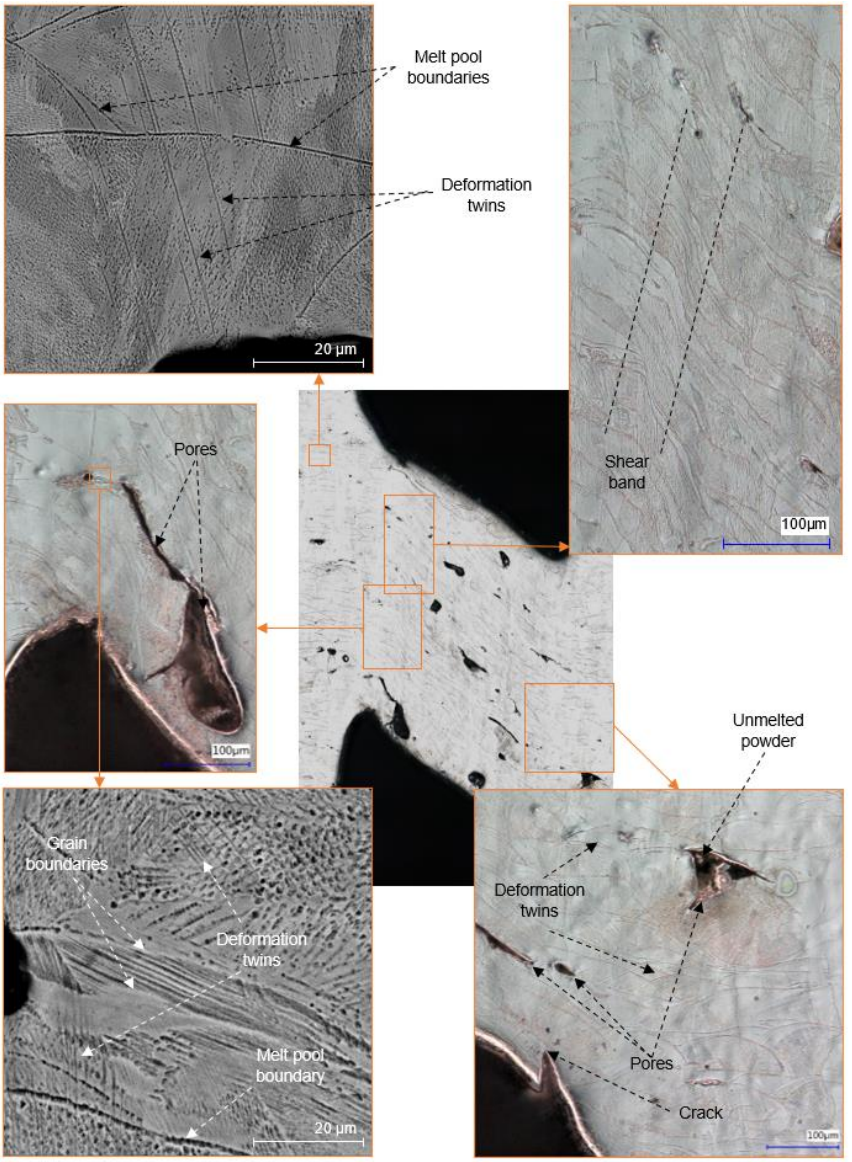

Fig. 18. Microstructure of sample No. 1 after the SHPB test

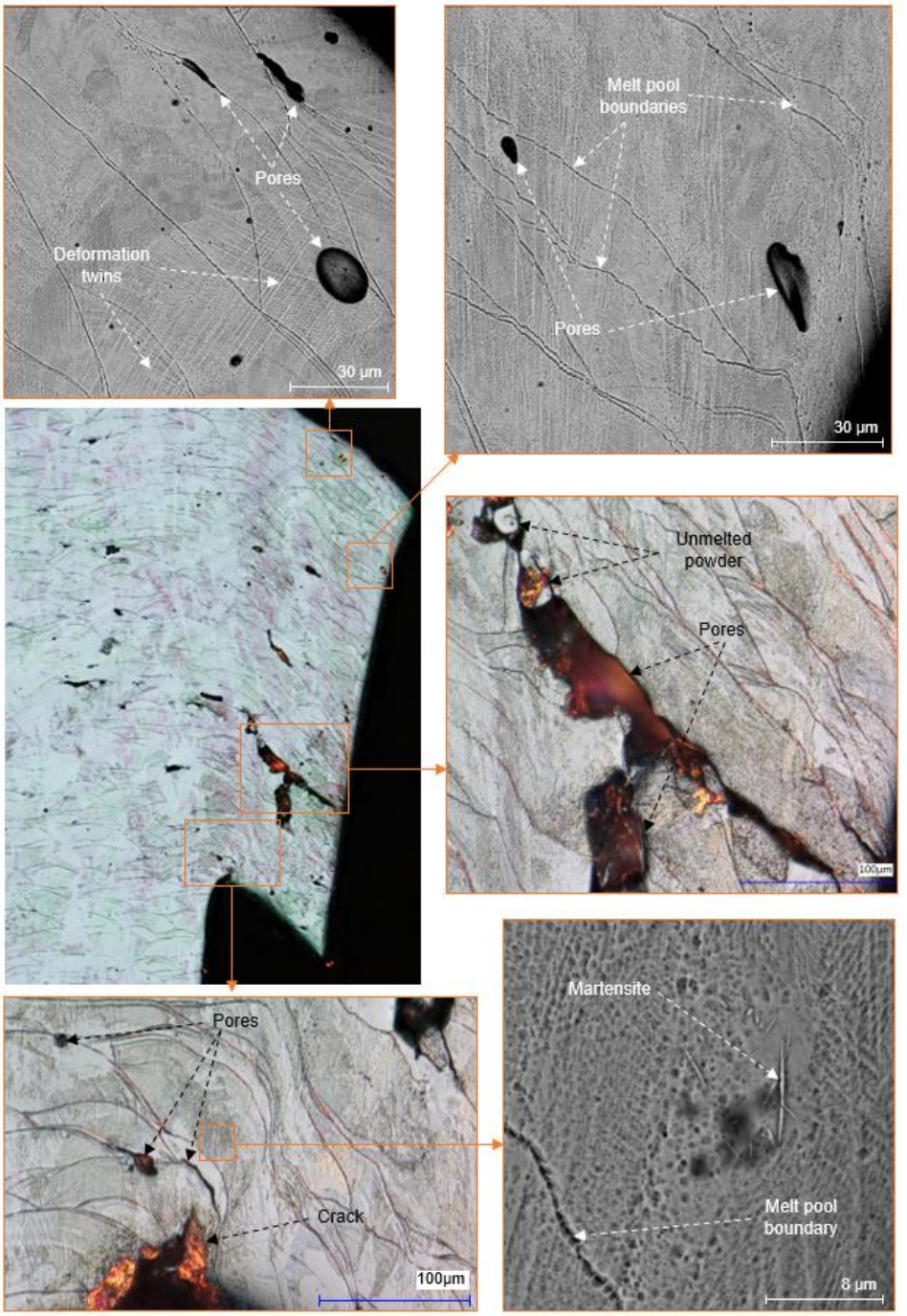

Fig. 19. Microstructure of sample No. 5 after the SHPB test

It is well known that in the case of the conventionally produced 316L steel exposed to dynamic deformation, the predominant deformation mechanism is twinning, which is favoured by a high deformation speed and low stacking fault energy for austenite. Moreover, the deformation of the developing twins indicates significant fragmentation of the grains and, in consequence, a strong strengthening of the material, leading to higher values of the plastic flow stress. Worth mentioning is that the increase in the plastic flow stress is associated with the increase in the strain rate, which is also caused by an increase in dislocation density. In our research, similar mechanisms were observed, together with the martensite transformation induced by higher strain rates.

4. CONCLUSIONS

Microstructural and mechanical characterisation of 316L samples, produced via the SLM method, has been presented. Tests carried out with the use of the SHPB method allowed us to determine the stress-strain curves. Recordings from a high-speed camera visualised the deformation process of the specimens and assisted with analysing the signals received from the strain gauges of the SHPB test rig. The presented results show the differences in the responses of specimens with different shear zones.

The microhardness of the samples, produced by the SLM method, was higher than conventionally produced 316L stainless steel in the annealed condition. It was also shown that the microhardness of the material increases with increasing plastic strain.

The analysis of the chemical composition of the samples showed compliance with the values specified in the standards, however, the test showed the uneven distribution of particular elements inside the material. Metallographic examination of the samples indicated that porosity at the top of the SLM samples is higher than at the bottom.

Microstructural analysis of impact-loaded areas revealed numerous defects. The main deformation mechanism appeared to be twinning. Large plastic deformations and many other microstructure changes such as shear bands, cracks and nucleation of martensite were also observed.

FUNDING

The authors received no financial support for the research, authorship, and/or publication of this article.

REFERENCES

[1] Brytan, Zbigniew. 2017. “Comparison of Vacuum Sintered and Selective Laser Melted Steel AISI 316L”. *Archives of Metallurgy and Materials* 62 (4) : 2125–2131.

[2] Li, Bolin, Tingting Wang, Peizhen Li, Shenghai Wang, and Li Wang. 2021. “Selective Laser Melting of 316L Stainless Steel: Influence of Co-Cr-Mo-W Addition on Corrosion Resistance”. *Metals* 11 (4) : 597-1-12.

[3] Zhai, Wengang, Wei Zhou, Zhiguang Zhu, and Sharon Mui Ling Nai. 2022. “Selective Laser Melting of 304L and 316L Stainless Steels: A Comparative Study of Microstructures and Mechanical Properties”. *Steel Research International* 93 (7) : 2100664.

[4] Röttger, Arne, Johannes Boes, W. Theisen, Magnus Thiele, and Cemal Esen. 2020. “Microstructure and mechanical properties of 316L austenitic stainless steel processed by different SLM devices”. *The International Journal of Advanced Manufacturing Technology* 108 (3) : 769–783.

[5] Bahl, Sumit, Sumeet Mishra, K.U. Yazar, Immanuel Raju Kola, Kaushik Chatterjee, and Satyam Suwas. 2019. “Non-equilibrium microstructure, crystallographic texture and morphological texture synergistically result in unusual mechanical properties of 3D printed 316L stainless steel”. *Additive Manufacturing* 28 : 65–77.

[6] Brytan, Zbigniew, Mirosław Bonek, Leszek Adam Dobrzański, Daniele Ugues, and Marco Actis Grande. 2010. “The Laser Surface Remelting of Austenitic Stainless Steel”. *Materials Science Forum* 654–656 : 2511–2514.

[7] Mertens A., S. Reginster, H. Paydas, Q. Contrepois, T. Dormal, O. Lemaire, and J. Lecomte-Beckers. 2014. “Mechanical properties of alloy Ti–6Al–4V and of stainless steel 316L processed by selective laser melting: influence of out-of-equilibrium microstructures”. *Powder Metallurgy* 57 (3) : 184–189.

[8] Liverani, E., S. Toschi, L. Ceschini, and A. Fortunato. 2017. “Effect of selective laser melting (SLM) process parameters on microstructure and mechanical properties of 316L austenitic stainless steel”. *Journal of Materials Processing Technology* 249 : 255–263.

[9] Yadroitsev, Igor, Pavel Krakhmalev, Ina Yadroitsava, Sten Å.H. Johansson, and I. Smurov. 2012. “Energy input effect on morphology and microstructure of selective laser melting single track from metallic powder,” *Journal of Materials Processing Technology* 213 (4) : 606–613.

[10] Yadollahi, Aref, Nima Shamsaei, Scott M. Thompson, and Denver W. Seely. 2015. “Effects of process time interval and heat treatment on the mechanical and microstructural properties of direct laser deposited 316L stainless steel”. *Materials Science and Engineering A* 644 : 171–183.

[11] Janiszewski, Jacek. 2012. *Badania materiałów inżynierskich w warunkach obciążenia dynamicznego*. Warszawa: Wydawnictwo Wojskowej Akademii Technicznej.
[12] Chen, Weinong, and Bo Song. 2011. *Split Hopkinson* (*Kolsky*) *Bar*. USA, Boston, MA: Springer.
[13] Kolsky, Herbert. 1964. "Stress waves in solids". *Journal of Sound and Vibration* 1 (1) : 88–110.
[14] Sreenivasan P.R., and S.K. Ray. 2001. Mechanical Testing at High Strain Rates. In *Encyclopedia of Materials: Science and Technology* 5269–5271. Elsevier.
[15] Zejian, Xu, Ding Xiaoyan, Zhang Weiqi, and Huang Fenglei. 2017. "A novel method in dynamic shear testing of bulk materials using the traditional SHPB technique". *International Journal of Impact Engineering* 101 : 90–104.
[16] Rusinek, Alexis, and J.R. Klepaczko. 2001. "Shear testing of a sheet steel at wide range of strain rates and a constitutive relation with strain-rate and temperature dependence of the flow stress". *International Journal of Plasticity* 17 (1) : 87–115.
[17] Meyer, W. Lothar, and Thorsten Halle. 2011. "Shear strength and shear failure, overview of testing and behavior of ductile metals". *Mechanics of Time-Dependent Materials* 15 (4) : 327–340.
[18] Saeidi, K., X. Gao, Y. Zhong, and Z. J. Shen. 2015. "Hardened austenite steel with columnar sub-grain structure formed by laser melting". *Materials Science and Engineering A* 625 : 221–229.
[19] Yadollahi, Aref, Denver Seely, Brian Patton, and Nima Shamsaei. 2015. "Microstructural Features and Mechanical Properties of 316L Stainless Steel fabricated by Laser Additive Manufacture". In *Proceedings of the 56th AIAA/ASCE/AHS/ASC Structures, Structural Dynamics, and Materials Conference*, 5-9 January 2015, Kissimmee, Florida, USA. DOI: 10.2514/6.2015-1355.
[20] Wang, Liang, and Sergio D. Felicelli. 2007. "Process Modeling in Laser Deposition of Multilayer SS410 Steel". *Journal of Manufacturing Science and Engineering* 129 (6) : 1028–1034.
[21] de Terris, Thibaut, Olivier Andreaua, Patrice Peyrea, Frédéric Adamskia, Imade Koutiria, Cyril Gornya, and Corinne Dupuya. 2019. "Optimization and comparison of porosity rate measurement methods of Selective Laser Melted metallic parts". *Additive Manufacturing* 28 : 802-813.
[22] Chen, Jie, Haiyang Wei, Kuo Bao, Xianfeng Zhang, Yang Cao, Yong Peng, Jian Kong, and Kehong Wang. 2021. "Dynamic mechanical properties of 316L stainless steel fabricated by an additive manufacturing process". *Journal of Materials Research and Technology* 11 : 70–179.

[23] Shen, Y.F., X.X. Li, X. Sun, Y.D. Wang, and L. Zuo. 2012. "Twinning and martensite in a 304 austenitic stainless steel". *Materials Science and Engineering: A* 552 : 514–522.

Dynamiczne zachowanie próbek ze stali 316L wytworzonych za pomocą metody SLM – właściwości mechaniczne i zmiany mikrostruktury

Paweł BIAŁOBRZEWSKI, Judyta SIENKIEWICZ,
Jacek JANISZEWSKI, Janusz KLUCZYŃSKI

Wojskowa Akademia Techniczna,
Wydział mechatroniki, Uzbrojenia i Lotnictwa
Instytut Techniki Uzbrojenia
ul. gen. Sylwestra Kaliskiego 2, 00-908 Warszawa

Streszczenie. Próbki ze stali 316L z trzema różnymi strefami ścinania wykonane metodą SLM (*Selective Laser Melting*) poddano testom dynamicznym wykorzystując do tego metodę dzielonego pręta Hopkinsona (*Split Hopkinson Pressure Bar*). Przeanalizowano wpływ odkształceń o dużej szybkości na zmiany w mikrostrukturze. Ponadto na podstawie wyników badań SHPB wyznaczono zależność naprężenie-odkształcenie. W celu zobrazowania procesu odkształcania próbek podczas badań zastosowano kamerę o dużej częstości klatkowania. Wykazano, że wraz ze wzrostem odkształcenia plastycznego wzrasta twardość materiału. Analiza mikrostrukturalna obszarów obciążonych dynamicznie ujawniła liczne defekty. Stwierdzono, że głównym mechanizmem deformacji jest bliźniakowanie. Zaobserwowano również duże odkształcenia plastyczne i wiele innych zmian mikrostruktury, takich jak pasma ścinania, pęknięcia i zarodkowanie martenzytu.
Słowa kluczowe: mikrostruktura, metody addytywne, SLM, stal nierdzewna, test dzielonego pręta Hopkinsona